Journal of Alloys and Compounds, 213/214 (1994) 93–99
JALCOM 4071

Oxidation of nuclear fuel (UO_2) by the products of water radiolysis: development of a kinetic model

H. Christensen[a], S. Sunder[b] and D.W. Shoesmith[b]
[a]*Studsvik Material AB, Nykoping (Sweden)*
[b]*AECL Research, Whiteshell Laboratories, Pinawa, Man. ROE 1LO (Canada)*

Abstract

Radiolysis of groundwater will produce oxidants and reductants which can affect the oxidation and dissolution of used fuel (UO_2) placed in a geological disposal vault. A kinetic model to describe the oxidation of UO_2 by the products of radiolysis of water is described. This model assumes that a monomolecular surface layer of UO_2 reacts as if it were dissolved in a thin layer of water of a thickness corresponding to the diffusion range of the radicals formed during radiolysis. In this manner we can use the rate constants for the reactions of radiolytic species with dissolved uranium as an analog of the heterogeneous system for which rate constants are unknown. The refinement of this model, based on a series of electrochemical and open-circuit corrosion experiments, is described. Model predictions are compared with dissolution rates measured in these experiments.

1. Introduction

In our attempts to predict the rate of release of radionuclides from used fuel disposed of in a nuclear waste vault, we have been trying to develop models that predict the effect of water radiolysis on the dissolution of uranium dioxide. We have reviewed existing models used to describe radionuclide release [1]. Here we describe our refinement of a kinetic model developed to predict the rate of UO_2 dissolution induced by water radiolysis. The mechanistic basis for these refinements is described briefly. The predicted dissolution (corrosion) rates are compared with rates determined using a previously published electrochemical model [2]. Finally, the limitations and necessary further developments are discussed.

2. Mechanism of oxidation and dissolution of uranium dioxide

The mechanism of oxidation and dissolution of UO_2 has been studied in detail electrochemically and under natural corrosion conditions [3–7]. The process that occurs under natural corrosion conditions is of interest here. A schematic diagram illustrating the general change in corrosion potential with time for neutral solutions, and indicating the progression in the oxidation and dissolution process with corrosion potential, is shown in Fig. 1. Many experimental curves exhibiting this general shape have been published [5, 6, 8–10]. The process can be divided into two distinct stages: (i) a transitory stage during which the surface is oxidized to approximately $UO_{2.33}$; (ii) a steady-state stage during which dissolution (as U^{VI}) occurs at a constant rate from a surface layer of $UO_{2.33}$ (5–8 nm thick). At sufficiently large oxidant concentrations, reprecipitation of U^{VI} to yield secondary phase ($UO_3 \cdot 2H_2O$) can occur [6].

We have commonly taken the time for the potential to reach a value of -100 mV (*vs.* SCE) as an approximate measure of the rate of formation of this $UO_{2.33}$ layer [11]. The appropriate corrosion (dissolution) rate is that obtained once steady-state dissolution conditions have been established, *i.e.* once $(E_{CORR})_{SS}$ has been attained (Fig. 1). At this potential the current for the oxidative dissolution of UO_2 is counterbalanced by an equal and opposite current for the oxidant reduction. It is this value of E_{CORR} which is used in our electrochemical model to obtain a value of corrosion rate. For dissolution in aerated solutions the rate-controlling step appears to be the reduction of oxygen, a notoriously slow reaction [12]. The first (of four) electron transfer appears to be the slow step. For radiolytic oxidants (O_2^-, OH, H_2O_2), electron transfer to the oxidant will be much faster, and the rate of the overall process is more likely to be controlled by the anodic dissolution step.

Elsevier Science S.A.
SSDI 0925-8388(94)04071-B

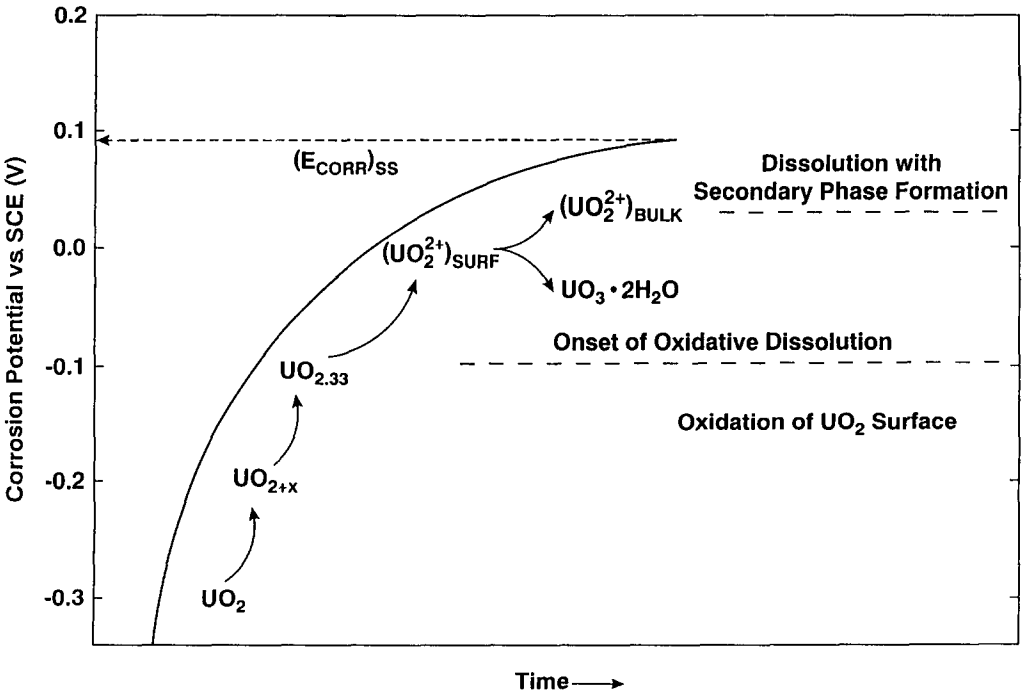

Fig. 1. Schematic diagram showing the behavior of the corrosion potential measured on UO_2 electrodes in 0.1 mol l^{-1} $NaClO_4$ (approximately pH 9.5). The stages of oxidation and dissolution are also illustrated.

3. Other experimental observations important in refining the model

(1) Electrochemical evidence indicates that the oxidation and dissolution reactions are irreversible under steady-state conditions [3–7, 13, 14].

(2) Dissolution occurs only in the +6 oxidation state [3, 13]. It is possible to envisage the $UO_{2.33}$ (U_3O_7) surface film as composed of either two U^{IV} and one U^{VI}, or two U^{V} and one U^{IV} species.

(3) The formation of the $UO_{2.33}$ surface film leads to a decrease in the oxidation rate as it thickens.

(4) Dissolved U^{VI} species diffuse out of the interfacial reaction zone into the bulk of the undersaturated solution, and hence are not reduced to any significant extent. The conclusion that the U^{VI} species, once formed, are not reduced to lower oxidation state species in ambient solutions has been shown by several electrochemical studies, see ref. 7 and references therein.

(5) Hydrogen peroxide has been observed to decompose on UO_2 surfaces [15] and electrochemical experiments indicate that decomposition of H_2O_2 predominates over dissolution of U^{VI} for peroxide concentrations up to 10^{-3} mol l^{-1} at pH 9.5 [1, 7].

(6) Experiments in solutions undergoing gamma radiolysis show that the rate of the film ($UO_{2.33}$) formation process depends on the nature and concentration of the oxidant (OH, O_2^-, H_2O_2 or O_2) [8–10].

4. Development of the kinetic model

Our model for UO_2 oxidation in solutions undergoing radiolysis is based on that originally proposed by Christensen and Bjergbakke [16]. To optimize this model for the neutral conditions expected in groundwaters, we have carried out experiments on the effects of water radiolysis on UO_2 oxidation in solutions of approximately pH 9.5.

The computer programs used in this model were designed for homogeneous reaction kinetics. Their adaptation to heterogeneous processes required the assumption that a monolayer of the UO_2 surface is reacting as if it were dissolved in a thin layer of water near the surface. The thickness of the water layer is assumed to be equal to the diffusion range $\bar{x}$ of the reacting radicals. This range is estimated from the calculated lifetime of radiolytically generated species at a specific dose rate [17]. For the OH radicals, $\bar{x}$ varies from 16 μm at a dose rate of 280 Gy h^{-1} to 44 μm at 5 Gy h^{-1}. Since this dependence of diffusion range on dose rate is only to the power -0.25 for the dose-rate range in our experiments, we have taken it to be constant at 25 μm. Thus, the initial concentration of UO_2 is set at a value of 5×10^{-4} mol l^{-1}, which corresponds to the dissolution of a monolayer of UO_2 in a water layer of thickness approximately 25 μm [16].

The rate constants for the reactions between radiolytic products are well established, as are the G values of the different species formed during radiolysis [18, 19].

Since the rate constants for reactions between radiolytic species and a solid UO_2 phase are unknown, we have adopted rate constants for the reaction of radiolytic species with other dissolved metallic species to represent the heterogeneous rate constants. Tables I and II in ref. 16 list the reactions and corresponding rate constants that formed the starting point in this model. The reactions and rate constants used in our refined model are given in Table 1. Here we discuss briefly the reasoning used in arriving at this refined model.

(a) The irreversibility of the overall oxidative dissolution process means that, under steady-state conditions, Fig. 1, the reduction of U^{VI} species is likely to be slow or negligible. Dissolved U^{VI} species are assumed to diffuse out of the reaction zone as UO_3D. A reaction was added to represent diffusion of UO_3 out of the reaction zone (reaction 56, Table 1).

(b) The reversible formation of U^V species (denoted UO_3H in Table 1) can be assumed to represent the reversible formation of the intermediate $UO_{2.33}$ film. This film reaches a steady-state thickness equivalent to a steady-state concentration of U^V in our model.

(c) Since $UO_{2.33}$ could equally well be envisaged as a mixture of U^{IV} and U^{VI} or as U^{IV} and U^V, the disproportionation reaction (reaction 36) could be considered most likely to occur within the surface film but not to lead to the formation of dissolved U^{VI} species, *i.e.* the rate constant for this reaction must be small compared with those for reactions leading to dissolution of U^{VI}.

(d) Owing to the formation of $UO_{2.33}$, the concentration of "available" U^{IV} decreases as steady state is approached. The arbitrary extent of this decrease is taken to be about a factor of 5 in concentration using dummy species UO_2D (reactions 59 and 60).

(e) The rate constants for oxidation by H_2O_2 reactions (reactions 33 and 39) were lowered relative to those for radicals in agreement with experimental observation [8].

(f) Reactions with arbitrary rate constants were added to represent decomposition of H_2O_2 on the UO_2 surface (*i.e.* reaction 50).

(g) Reactions to represent the slow oxidation of UO_2 by dissolved O_2 in the absence of a radiation field [5, 6] were added (reactions 57 and 58).

(h) The experimental rates with which the predictions of this model are to be compared were determined in an open system making it necessary to include rate constants for the removal of gases (O_2, H_2) from the system (reactions 48 and 49).

5. Comparison of model predictions with experimental results

Model calculations were carried out using the computer program MAKSIMA-CHEMIST [20], and these calculations are compared with results from electrochemical experiments in Tables 2 and 3.

Table 2 compares the times taken to reach 90% of the steady-state concentration of UO_3H species with the experimental times to reach an open-circuit (OC) corrosion potential of -100 mV. Table 3 compares the calculated and experimental corrosion (dissolution) rates for UO_2. Experimental corrosion rates were obtained from values of $(E_{CORR})_{SS}$ using our electrochemistry-based model [1, 2]. Calculated dissolution rates were obtained from concentration–time profiles predicted by the model. Figure 2 shows two such sets of calculated profiles for argon-purged solutions, at initial pH 9.5, undergoing gamma radiolysis at dose rates of 5 and 280 Gy h^{-1} respectively. Dissolution rates were obtained from the linear increase in dissolved U^{VI} (UO_3D) over the period 20–30 h, as indicated in Fig. 2.

6. Summary and conclusions

The important features of our experiments are present in the profiles in Figs. 2(a) and 2(b). The concentration of U^V (UO_3H), taken as an indication of formation of the intermediate film ($U^{IV}\,U_2^V\,O_7$), eventually reaches a steady-state value. This value is achieved over the same time interval for which steady-state dissolution is predicted, *i.e.* UO_3D increases linearly with time. This behavior simulates our experimental finding that dissolution occurs from a film of constant thickness. The steady-state concentration of U^V (UO_3H) is, however, low and equivalent to substantially less than a monolayer if considered as a film. This observation is at odds with our experimental finding, showing this layer to be 5–8 nm thick, equivalent to tens of monolayers [5, 6, 9, 10].

It is possible that this low concentration of U^V (UO_3H) reflects the relatively small decrease in the concentration of "available" UO_2 as a consequence of coverage by the intermediate U^V (UO_3H). Experimental evidence suggests that inhibition of the overall oxidative dissolution rate by the formation of $UO_{2.33}$ is much greater.

The predicted concentration of U^V (UO_3H-($\equiv UO_{2.33}$) $\equiv$ layer thickness) is approximately a factor of 5 lower at a dose rate of 5 Gy h^{-1} compared with 280 Gy h^{-1}, Fig. 2. This is in qualitative agreement with experimental observation. At 5 Gy h^{-1} the corrosion potential did not achieve a value of -100 mV in deoxygenated solutions [10] and, consequently, the thickness of the $UO_{2.33}$ layer would be less than the steady-state thickness.

For high dose rates the model predicts quite accurately the rate of oxidation of the UO_2 surface to $UO_{2.33}$, *i.e.* the predicted time to reach 90% of the steady-state

TABLE 1. Reaction mechanism of UO_2 oxidation

Number	Reaction[a]	Rate constant[b]
1	$OH + H_2 = H + H_2O$	$k_1 = 3.400 \times 10^7$
2	$OH + H_2O_2 = HO_2 + H_2O$	$k_2 = 2.700 \times 10^7$
3	$OH + O_2^- = O_2 + OH^-$	$k_3 = 9.000 \times 10^9$
4	$H + O_2 = HO_2$	$k_4 = 1.800 \times 10^{10}$
5	$H + O_2^- = HO_2^-$	$k_5 = 2.000 \times 10^{10}$
6	$e^- + O_2 = O_2^-$	$k_6 = 1.900 \times 10^{10}$
7	$e^- + H_2O_2 = OH + OH^-$	$k_7 = 1.200 \times 10^{10}$
8	$e^- + O_2^- = HO_2^- + OH^- - H_2O$	$k_8 = 1.300 \times 10^{10}$
9	$e^- + H^+ = H$	$k_9 = 2.200 \times 10^{10}$
10	$e^- + H_2O = H + OH^-$	$k_{10} = 2.000 \times 10^1$
11	$e^- + HO_2^- = O^- + OH^-$	$k_{11} = 3.500 \times 10^9$
12	$OH + HO_2 = H_2O + O_2$	$k_{12} = 7.900 \times 10^9$
13	$OH + OH = H_2O_2$	$k_{13} = 5.500 \times 10^9$
14	$H + HO_2 = H_2O_2$	$k_{14} = 2.000 \times 10^{10}$
15	$H + H_2O_2 = H_2O + OH$	$k_{15} = 6.000 \times 10^7$
16	$H + OH^- = e^- + H_2O$	$k_{16} = 1.500 \times 10^7$
17	$HO_2 + O_2^- = O_2 + HO_2^-$	$k_{17} = 9.600 \times 10^7$
18	$HO_2 + HO_2 = H_2O_2 + O_2$	$k_{18} = 8.400 \times 10^5$
19	$H^+ + O_2^- = HO_2$	$k_{19} = 4.500 \times 10^{10}$
20	$HO_2 = H^+ + O_2^-$	$k_{20} = 8.000 \times 10^5$
21	$H^+ + HO_2^- = H_2O_2$	$k_{21} = 2.000 \times 10^{10}$
22	$H_2O_2 = H^+ + HO_2^-$	$k_{22} = 3.560 \times 10^{-2}$
23	$OH + OH^- = H_2O + O^-$	$k_{23} = 1.200 \times 10^{10}$
24	$O^- + H_2O = OH + OH^-$	$k_{24} = 9.300 \times 10^7$
25	$H^+ + OH^- = H_2O$	$k_{25} = 1.430 \times 10^{11}$
26	$H_2O = H^+ + OH^-$	$k_{26} = 2.574 \times 10^{-5}$
27	$e^- + OH = OH^-$	$k_{27} = 3.000 \times 10^{10}$
28	$H + OH = H_2O$	$k_{28} = 2.000 \times 10^{10}$
29	$H + H = H_2$	$k_{29} = 1.000 \times 10^{10}$
30	$e^- + H = H_2 + OH^- - H_2O$	$k_{30} = 2.500 \times 10^{10}$
31	$OH + HO_2^- = HO_2 + OH^-$	$k_{31} = 5.000 \times 10^9$
32	$UO_2 + OH = UO_3H$	$k_{32} = 4.000 \times 10^8$
33	$UO_2 + H_2O_2 = UO_3H + OH$	$k_{33} = 2.000 \times 10^{-1}$
34	$UO_2 + HO_2 = UO_3H + H_2O_2 - H_2O$	$k_{34} = 2.000 \times 10^8$
35	$UO_2 + O_2^- = UO_3H + HO_2^- - H_2O$	$k_{35} = 2.000 \times 10^8$
36	$UO_3H + UO_3H = UO_3 + UO_2 + H_2O$	$k_{36} = 1.000 \times 10^{-1}$
37	$UO_3H + OH = UO_3 + H_2O$	$k_{37} = 8.000 \times 10^8$
38	$UO_3H + e^- = UO_2 + OH^-$	$k_{38} = 5.000 \times 10^8$
39	$UO_3H + H_2O_2 = UO_3 + H_2O + OH$	$k_{39} = 2.000 \times 10^{-1}$
40	$UO_3H + O_2^- = UO_3 + HO_2^-$	$k_{40} = 4.000 \times 10^8$
41	$UO_3H + HO_2 = UO_3 + H_2O_2$	$k_{41} = 4.000 \times 10^8$
42	$UO_3 + e^- = UO_3H + OH^- - H_2O$	$k_{42} = 5.000 \times 10^8$
43	$UO_3 + O_2^- = UO_3^- + O_2$	$k_{43} = 4.000 \times 10^7$
44	$UO_3^- + H_2O = UO_3H + OH^-$	$k_{44} = 1.000 \times 10^1$
45	$UO_3H + H = UO_2 + H_2O$	$k_{45} = 4.500 \times 10^6$
46	$UO_3 + H = UO_3H$	$k_{46} = 4.500 \times 10^6$
47	$UO_3 + HO_2 = UO_3H + O_2$	$k_{47} = 4.000 \times 10^7$
48	$O_2 = O_2D$	$k_{48} = 2.100 \times 10^{-1}$
49	$H_2 = H_2D$	$k_{49} = 3.500 \times 10^{-1}$
50	$H_2O_2 = H_2O + O$	$k_{50} = 1.000 \times 10^{-3}$
51	$O + O = O_2$	$k_{51} = 1.000 \times 10^9$
52	$N_2O + e^- = N_2 + OH + OH^- - H_2O$	$k_{52} = 6.000 \times 10^9$
53	$HCOOK + OH = CO_2^- + H_2O + K^+$	$k_{53} = 2.000 \times 10^9$
54	$CO_2^- + O_2 = O_2^- + CO_2$	$k_{54} = 6.000 \times 10^9$
55	$CO_2 + H_2O = HCO_3^- + H^+$	$k_{55} = 1.000 \times 10^3$
56	$UO_3 = UO_3D$	$k_{56} = 4.000 \times 10^{-4}$
57	$UO_2 + O_2 = UO_3H + HO_2 - H_2O$	$k_{57} = 1.000 \times 10^{-3}$
58	$UO_3H + O_2 = UO_3 + HO_2$	$k_{58} = 1.000 \times 10^{-3}$
59	$UO_2 = UO_2D$	$k_{59} = 7.000 \times 10^{-4}$
60	$UO_2D = UO_2$	$k_{60} = 3.500 \times 10^{-7}$

[a] UO_3D represents UO_3 diffusing out of the reaction layer near the UO_2 surface (reaction 56), see text (Section 3.4); UO_2D represents a dummy species used to maintain the supply of UO_2 in the reaction layer (reactions 59 and 60), see ref. 16.

[b] Rates are in units of $(\text{mol l})^{-1}\ \text{s}^{-1}$ for second-order reactions; reaction rates are for room temperature.

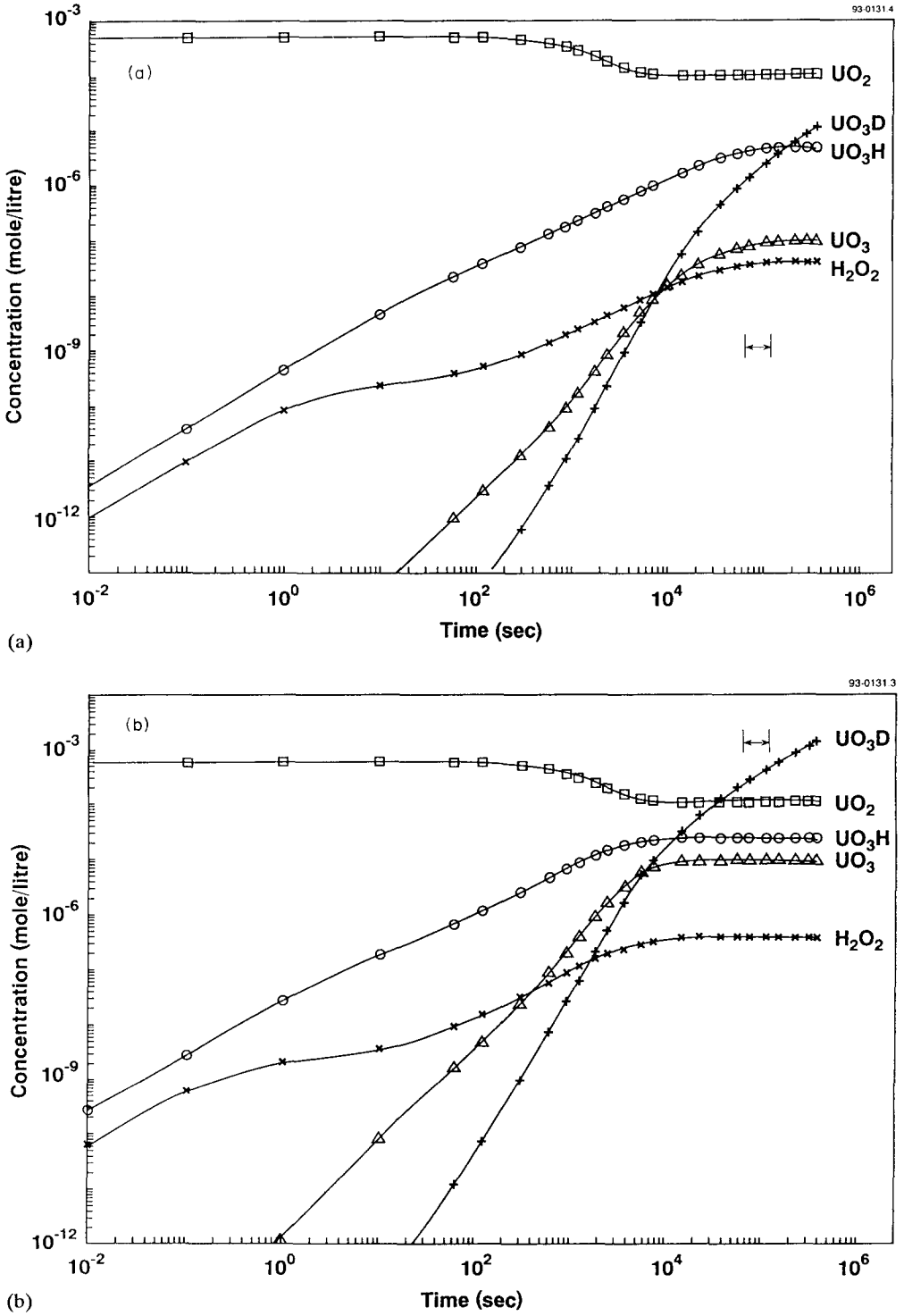

Fig. 2. Concentration of selected radiolysis products in solutions with UO_2 and undergoing gamma radiolysis; Ar-purged water, pH 9.5, dose rate (a) 5 Gy h^{-1} and (b) 280 Gy h^{-1}. Arrows define the period over which the dissolution rates were measured.

concentration of U^V (UO_3H) is in good agreement with the experimental time to reach -100 mV, Table 2. However, the agreement at low dose rates, and especially in the absence of radiolysis when only O_2 and H_2O_2 are present, is not so good.

The agreement between calculated and electrochemically measured corrosion (dissolution) rates is generally good, Table 3. It should be noted that significant uncertainty is associated with the extrapolation required to calculate dissolution rates from electrochemical data

TABLE 2. Comparison of experimental and calculated times for the formation of a $UO_{2.33}$ film on UO_2

Solution[a]	Dose rate (Gy h^{-1})	Time (h)	
		Calculated[b]	Experimental[c]
Ar-purged	5	25	19
Ar-purged	280	2	2
N_2O-purged	5	25	9
N_2O-purged	280	0.2	0.5
O_2-purged	5	20	1.6
O_2-purged	280	0.2	0.15
O_2-purged	0	50	3
H_2O_2 10^{-6} mol l^{-1}	0	80	8
H_2O_2 2×10^{-4} mol l^{-1}	0	1.5	0.02

[a]Base solution is 0.1 mol l^{-1} $NaClO_4$, pH 9.5.
[b]Time to reach 90% steady-state concentration of UO_3H species.
[c]Time taken to reach a corrosion potential of -100 mV *vs.* SCE.

TABLE 3. Comparison of calculated and experimental corrosion rates

Solution[a]	Dose rate (Gy h^{-1})	Corrosion rate[b]	
		Calculations	Experiments
Ar-purged	5	0.003	8×10^{-5}
Ar-purged	280	0.12	0.10
N_2O-purged	5	0.04	8×10^{-5}
N_2O-purged	280	0.84	0.36
O_2-purged	5	0.06	0.13
O_2-purged	280	0.84	0.75
O_2-purged	0	2.3×10^{-2}	3.8×10^{-3}
H_2O_2 $\times10^{-6}$ M	0	8.0×10^{-4}	2.1×10^{-4}
H_2O_2 2×10^{-4} M	0	1.4	0.13

[a]Base solution is 0.1 mol l^{-1} $NaClO_4$, pH 9.5.
[b]Corrosion rate in $\mu g\ cm^{-2}\ d^{-1}$.

[1, 2]. The largest discrepancy between measured and predicted rates in irradiated solutions is for measurements in N_2O-purged solutions. In this case, the experimental values are suspect owing to unusual behavior of potential–time curves [10].

The discrepancy observed between measured and calculated corrosion rates for H_2O_2 solutions in the absence of radiolysis is large, Table 3, especially at the higher H_2O_2 concentrations. Our experimental evidence suggests UO_2 is subject to redox buffering by peroxide decomposition which involves the simultaneous oxidation and reduction of H_2O_2 [1, 7]. Reaction 50, Table 1, does not account for this process adequately, leading to a predicted increase in dissolution rate with H_2O_2 concentration which is not observed experimentally. The ability of the UO_2 surface to catalyze this process appears to change with composition, making it difficult to incorporate into our model.

This model possesses a number of deficiencies which will be difficult to accommodate. In particular, (i) the model is insensitive to surface structure and composition and therefore cannot account for observed differences in reactivity for different specimens of UO_2, and (ii) the potential dependence of rate constants for heterogeneous charge transfer (electrochemical) reactions cannot be incorporated. These deficiencies may be less apparent for steady-state conditions when experiments suggest a similar reactivity for all surfaces owing to the common presence of the $UO_{2.33}$ film. Additional experiments to obtain further information about the effects of surface reactivity on the reactions of radiolysis products with UO_2 fuel are in progress.

Acknowledgments

We thank N.H. Sagert and J.C. Tait for helpful comments on the manuscript. This work was done under the Canadian Nuclear Fuel Waste Management Program, which is funded jointly by AECL Research and Ontario Hydro under the auspices of the CANDU Owners Group. H. Christensen acknowledges support from SKB of Sweden. AECL-11020, COG-93-478.

References

1 D.W. Shoesmith and S. Sunder, An electrochemistry-based model for the dissolution of UO_2, *SKB Tech. Rep., 91-63*, Stockholm, 1991; also published as *AECL-10488*, 1991 (Atomic Energy of Canada Ltd.), Pinawa, Canada.
2 D.W. Shoesmith and S. Sunder, *J. Nucl. Mater., 190* (1992) 20.
3 S. Sunder, D.W. Shoesmith, M.G. Bailey, F.W. Stanchell and N.S. McIntyre, *J. Electroanal. Chem., 130* (1981) 163.
4 D.W. Shoesmith, S. Sunder, M.G. Bailey, G.J. Wallace and F.W. Stanchell, *Appl. Surf. Sci., 20* (1984) 39.
5 D.W. Shoesmith, S. Sunder, M.G. Bailey and G.J. Wallace, *Corros. Sci., 29* (1989) 1115.
6 S. Sunder, D.W. Shoesmith, R.J. Lemire, M.G. Bailey and G.J. Wallace, *Corros. Sci., 32* (1991) 373.
7 S. Sunder and D.W. Shoesmith, Chemistry of UO_2 fuel dissolution in relation to the disposal of used nuclear fuel, *AECL-10395*, 1991 (Atomic Energy of Canada Limited), Pinawa, Canada.
8 S. Sunder, D.W. Shoesmith, H. Christensen, M.G. Bailey and N.H. Miller, *Mater. Res. Soc. Symp. Proc., 127* (1989) 317.
9 S. Sunder, D.W. Shoesmith, H. Christensen, N.H. Miller and M.G. Bailey, *Mater. Res. Soc. Symp. Proc., 176* (1990) 457.
10 S. Sunder, D.W. Shoesmith, H. Christensen and N.H. Miller, *J. Nucl. Mater., 190* (1992) 78.
11 S. Sunder, D.W. Shoesmith, N.H. Miller and G.J. Wallace, *Mater. Res. Soc. Symp. Proc., 257* (1992) 345.

12 W.H. Hocking, J.S. Betteridge and D.W. Shoesmith, The cathodic reduction of dioxygen on uranium oxide in dilute alkaline aqueous solution, *AECL-10402,* 1991 (Atomic Energy of Canada Limited), Pinawa, Canada.
13 M.J. Nicol and C.R.S. Needes, *Electrochim. Acta, 20* (1975) 585.
14 M.J. Nicol and C.R.S. Needes, *Electrochim. Acta, 22* (1977) 1381.
15 H. Christensen, R.S. Forsyth, R. Lundqwist and L.O. Werme, Radiation-induced dissolution of UO_2, *Studsvik Nuclear Rep. No. NS-90/85,* 1990, Studsvik, Sweden.
16 H. Christensen and E. Bjergbakke, *Mater. Res. Soc. Symp. Proc., 84* (1987) 115.
17 H. Christensen and S. Sunder, Calculations of radiolysis in connection with UO_2 oxidation studies, *Studsvik Nuclear Rep. No. NS-89/117,* 1989, Studsvik, Sweden.
18 E. Bjergbakke, K. Sehested, O.L. Rasmussen and H. Christensen, Input files for computer simulation of water radiolysis, *Riso-M-2430,* 1984 (Riso National Laboratory, DK4000 Roskilde).
19 G.V. Buxton, C.L. Greenstock, W.P. Helmand and A.B. Ross, *J. Phys. Chem. Ref. Data, 17* (1988) 513.
20 M.B. Carver, D.V. Hanley and K.R. Chaplin, MAKSIMA-CHEMIST, a program for mass action kinetics simulation by automatic chemical equation manipulation and integration using stiff techniques, *AECL-6413,* 1979 (Atomic Energy of Canada Limited), Pinawa, Canada.